NIH Public Access
Author Manuscript
J Biomech. Author manuscript; available in PMC 2009 March 16.

Published in final edited form as:
J Biomech. 2007 ; 40(8): 1686–1693. doi:10.1016/j.jbiomech.2006.09.004.

ENGINEERING CONTROLLABLE ANISOTROPY IN ELECTROSPUN BIODEGRADABLE NANOFIBROUS SCAFFOLDS FOR MUSCULOSKELETAL TISSUE ENGINEERING

Wan-Ju Li,
Cartilage Biology and Orthopaedics Branch, National Institute of Arthritis and Musculoskeletal and Skin Diseases, National Institutes of Health, Bethesda, MD

Robert L. Mauck[^],
Cartilage Biology and Orthopaedics Branch, National Institute of Arthritis and Musculoskeletal and Skin Diseases, National Institutes of Health, Bethesda, MD

James A. Cooper,
Polymers Division, National Institute of Standards and Technology, Rockville, MD

Xiaoning Yuan, and
Cartilage Biology and Orthopaedics Branch, National Institute of Arthritis and Musculoskeletal and Skin Diseases, National Institutes of Health, Bethesda, MD

Rocky S. Tuan[‡]
Cartilage Biology and Orthopaedics Branch, National Institute of Arthritis and Musculoskeletal and Skin Diseases, National Institutes of Health, Bethesda, MD

Abstract

Many musculoskeletal tissues exhibit significant anisotropic mechanical properties reflective of a highly oriented underlying extracellular matrix. For tissue engineering, recreating this organization of the native tissue remains a challenge. To address this issue, this study explored the fabrication of biodegradable nanofibrous scaffolds composed of aligned fibers via electrospinning onto a rotating target, and characterized their mechanical anisotropy as a function of the production parameters. The characterization showed that nanofiber organization was dependent on the rotation speed of the target; randomly oriented fibers (33% fiber alignment) were produced on a stationary shaft, whereas highly oriented fibers (94% fiber alignment) were produced when rotation speed was increased to 9.3 m/sec. Non-aligned scaffolds had an isotropic tensile modulus of 2.1 ± 0.4 MPa, compared to highly anisotropic scaffolds whose modulus was 11.6 ± 3.1 MPa in the presumed fiber direction, suggesting that fiber alignment has a profound effect on the mechanical properties of scaffolds. Mechanical anisotropy was most pronounced at higher rotation speeds, with a greater than 33-fold enhancement of the Young's modulus in the fiber direction compared to perpendicular to the fiber direction at a rotation speed reached 8 m/sec. In cell culture, both the organization of actin filaments of human mesenchymal stem cells and the cellular alignment of meniscal fibroblasts were dictated

‡**Corresponding Author:** Rocky S. Tuan, Ph.D., Branch Chief, Cartilage Biology and Orthopaedics Branch, National Institute of Arthritis and Musculoskeletal and Skin Diseases, National Institutes of Health, 50 South Drive, MSC 8022, Building 50, Room 1503, Bethesda, MD 20892-8022, Phone: (301) 451-6854, Fax: (301) 480-4315, Email: tuanr@mail.nih.gov.
[^]Present address: McKay Orthopaedic Research Laboratory, Department of Orthopaedic Surgery, University of Pennsylvania, Philadelphia, PA

Publisher's Disclaimer: This is a PDF file of an unedited manuscript that has been accepted for publication. As a service to our customers we are providing this early version of the manuscript. The manuscript will undergo copyediting, typesetting, and review of the resulting proof before it is published in its final citable form. Please note that during the production process errors may be discovered which could affect the content, and all legal disclaimers that apply to the journal pertain.

NIH-PA Author Manuscript
NIH-PA Author Manuscript
NIH-PA Author Manuscript

NIH-PA Author Manuscript

NIH-PA Author Manuscript

NIH-PA Author Manuscript

by the prevailing nanofiber orientation. This study demonstrates that controllable and anisotropic mechanical properties of nanofibrous scaffolds can be achieved by dictating nanofiber organization through intelligent scaffold design.

Keywords

Tissue Engineering; Tensile Properties; Anisotropy; Mechanical Testing; Biodegradable Scaffolds

1. Introduction

Damage to the soft tissues of the musculoskeletal system often result in failure to repair or the formation of regenerate tissue of inferior mechanical quality. To augment healing, tissue engineering creates replacements via the combination of cells with biocompatible scaffolds. One recent fabrication technique for the creation of scaffolds involves the production of nanofibrous meshes via electrospinning (Li et al., 2002). Nanofibrous scaffolds produced by electrospinning are considerably smaller than the micro-fibers produced using conventional extrusion techniques, and are similar in size scale to elements of the native extracellular matrix (ECM) (Li et al., 2003; Riesle et al., 1998).

When formed as random mats, nanofibrous scaffolds exhibit isotropic mechanical properties reflective of their polymer composition (Li et al., 2006; Tan et al., 2005). For example, we have recently shown that while poly(D,L-lactic-co-glycolic acid 50:50) produce nanofibrous meshes that are quite stiff, plastic deformation occurs with little elongation. Conversely, scaffolds composed of poly-ε-caprolactone (PCL) are 10 times less stiff, but remain elastic over a wider range (Li et al., 2006).

While randomly oriented nanofibrous scaffolds support neo-tissue formation, many tissues in the musculoskeletal system, particularly those that bear mechanical load in a defined direction, exhibit preferential fiber alignment. This alignment endows such tissues with functional properties that vary depending on the testing direction. For example, in tendons and ligaments, tensile properties are 200–500 times higher along compared to perpendicular to the fiber direction (Lynch et al., 2003). In articular cartilage, tensile properties are greatest in the superficial zone along the split line direction (Huang et al., 1999; Mow and Guo, 2002; Woo et al., 1976). In the meniscus, circumferentially oriented collagen fibers predominate (Petersen and Tillmann, 1998), resulting in higher tensile properties in the circumferential compared to the radial direction (Fithian et al., 1990; Proctor et al., 1989; Setton et al., 1999).

Our goal in engineering musculoskeletal tissues is to recapitulate the functional properties of these complex structures, including their structural anisotropy. We therefore investigated a new technique for creating anisotropy in nanofibrous scaffolds to create a 3-dimensional micro-pattern to guide tissue formation. In this study, we describe a method for creating anisotropic nanofibrous scaffolds by incorporating a rotating target onto which fibers are deposited. We characterize the organization and mechanical properties of these structures, and their dependence on production parameters. Furthermore, we develop a simple model to understand the relationship between fiber angle and measured mechanical properties. Finally, we examine the short-and long-term polarity of cells commonly used in musculoskeletal tissue engineering (mesenchymal stem cells and meniscal fibrochondrocytes) on these fiber-aligned nanofibrous scaffolds.

NIH-PA Author Manuscript

NIH-PA Author Manuscript

NIH-PA Author Manuscript

2. Materials and Methods

2.1. Scaffold fabrication

PCL scaffolds were produced via electrospinning (Li et al., 2003). Briefly, PCL (Sigma Chemicals, St. Louis, MO, 80 kD, ρ=1.145 g/cm^3) was dissolved in a 1:1 mixture of tetrahydrofuran:N,N-dimethylformamide at 0.14g/mL. Polymer was drawn through an 18 gauge metal needle with a 15 kV potential (Gamma High Voltage, Ormand Beach, FL, ES30-5W) through a distance of 20 cm. To direct alignment, a rotating target (1" aluminum rod covered with aluminum foil or with attached Superfrost glass slides) was placed in the path of the polymer jet (see Fig. 1). The rod was connected to an AC motor controlled by a rheostat (Variac, Cleveland, OH). Rotation speed was calibrated using a phototachometer (TIF, Lynn Haven, FL). For characterization of alignment, a range of speeds were analyzed (0–7000 rpm, 0–9.3 m/s). For mechanical testing and cellular attachment studies, scaffolds were formed on two separate occasions at four speeds: 0, 0.3, 4, and 8 m/s.

2.2. Electron microscopy and characterization of fiber orientation

To visualize fibers, scaffolds were viewed by scanning electron microscopy (JEOL, JSM-5300,). Fiber alignment was assessed on images using Image J (1.30v, National Institutes of Health, Bethesda, MD). Ten equally spaced vertical lines (5 pixel width) were superimposed on each image. Beginning from the left periphery, fiber orientation with respect to the vertical line was determined for each line/fiber intersection. Between 300–400 points were measured in each image, with the mean angle subtracted from the population to normalize the alignment of the scaffold within the imaging chamber. Histograms of this data were plotted over the entire +90° to −90° range. The percentage of fibers within a region within ±20° of the prevailing fiber direction was calculated.

2.3. Mechanical testing

Uni-axial tensile testing was carried out on scaffolds ranging in thickness from 0.7–1.0 mm. Strips were excised at 4 cm length × 0.5 cm width parallel (in the direction of rotation) or perpendicular to the presumed fiber direction. Mechanical testing was performed using a custom apparatus (Mauck et al., 2000; Soltz and Ateshian, 1998; Soltz and Ateshian, 2000) consisting of a stepper micrometer (Oriel Instruments, Stratford, CT,) in series with an LVDT (Schaevitz Sensors, Hampton, VA) and 10 lb load cell (Sensotec, Columbus, OH). For testing, scaffolds were fitted into grips (Ametek, Brooklyn, NY) coated with 80-grit sandpaper. Sample dimensions and weight were measured prior to each test, and apparent density calculated. Scaffolds were preconditioned with 10 sinusoidal cycles of 0.5% strain at 0.1Hz. Tensile tests (up to ~70% elongation) were carried out at a constant strain rate of 0.1%/s. Tensile modulus was calculated from the linear region of the stress-strain curve (0–2% for perpendicular (weaker) scaffolds and 5–10% for parallel (stronger) scaffolds), and ultimate strain noted when samples failed at or below the ~70% applied strain. For all samples, the yield stress and strain were determined from the intersection of a line parallel to the linear region offset by +0.5% strain. Six to eight samples were tested for each group, with properties reported as the mean ± SD.

2.4. Mesenchymal stem cell and meniscal fibrochondrocyte culture

To visualize cell morphology, scaffolds were UV sterilized and pre-wet with fetal bovine serum (FBS) for 30 minutes. Passage two human mesenchymal stem cells (hMSCs), obtained from patients (Haynesworth et al., 1992; Noth et al., 2002) undergoing elective total joint replacement according to IRB-approved protocol (George Washington University), were cultured on scaffolds in 20 μl drops at a density of 2.5×10^5 cells/mL. After 4 hours, constructs were flooded with Dulbecco's Modified Eagle's Medium (DMEM) containing 10% FBS and

NIH-PA Author Manuscript

NIH-PA Author Manuscript

NIH-PA Author Manuscript

1X penicillin/streptomycin/Fungizone (PSF). After 8, 24, and 72 hours of culture, constructs were washed with phosphate-buffered saline (PBS) and fixed for 20 min in 4% paraformaldehyde and permeabilized for 5 min at 4°C with 0.5% Triton X in PBS, containing 10% sucrose and 3 mM $MgCl_2$. Filamentous actin was labeled with TRITC-phalloidin (1:1000 in 1%BSA-PBS) for 1 hour at 37°C. Constructs were imaged using confocal microscopy.

To assess long-term cell alignment, meniscal fibrochondrocytes isolated from calf (3–6 month old) menisci by overnight digestion were expanded through passage two. Prior to culture, scaffolds were sterilized and rehydrated and incubated in DMEM containing 10% FBS and 1X PSF. Fifty microliter aliquots containing 300,000 cells were loaded onto each scaffold four times (twice per side) at 30 min intervals. Cell viability and shape were assessed on days 1 and 28 using the Live/Dead assay (Molecular Probes, Eugene, OR).

2.5. Fiber dispersion model of scaffold mechanical properties

To better understand the mechanical characteristics of fiber-aligned scaffolds, an elastic spring model was formulated. Each scaffold was prescribed dimensions of 1 unit width (y-direction) by four unit length (x-direction) based on the width of the tested scaffolds (0.5 cm) and the approximate gauge length (2 cm). One hundred nanofibers were generated within this scaffold space, each with a random starting position along the unit width (y_i). Each fiber was assigned a random angle (θ_i) with respect to the long axis bounded by the restriction that they fall within an allowable range (0° to ± 90° in ±5° increases per step). Each fiber was treated as a spring element with a characteristic stiffness (k) equal to unity. For each dispersion scenario, the apparent stiffness of the scaffold in the testing direction ($K_{\text{app}}=\sum_{i=1}^{100} k \times \cos\theta_i \times \Omega(y_i,\theta_i)$) was calculated with two different assumptions: i) Free model: fibers that exit over the length of the mesh do not contribute to the apparent stiffness ($\Omega(y_i, \theta_i)$= 1 or 0, depending on the fiber angle θ_i and starting position y_i) and ii) Bound model: junctions or entanglements between fibers result in each fiber contributing to the apparent stiffness (Ω=1). For each range of allowable angles, K_{app} was calculated for the Free and Bound case, with the average valued derived from 10 iterations of randomized starting position and angle. To compare experimental data to this model, the percentage of fibers in the model falling within ±20° was determined for each allowable angle step. These data were fit with a power law curve (R^2=0.998) and the allowable angles in measured scaffolds defined according to this relationship. The mechanical properties of measured scaffolds (parallel samples produced at 0, 0.3, 4.0, and 8.0 m/s) were then plotted along with the model predictions.

2.6. Statistical analysis

Analysis of variance (ANOVA) was carried out using SYSTAT (v10.2, Port Richmond, CA). Dependent variables included the apparent density, Young's modulus, and yield stress and strain. Independent variables included target speed and direction of testing. When significance was found, a Fisher's least significant difference posthoc test was performed to make comparisons between groups, with $p<0.05$

3. Results

This study demonstrates increased fiber alignment when electrospinning is carried out with a moving target. Electrospinning of a PCL solution onto a static surface resulted in a random nanofibrous mesh with no particular fiber orientation (Fig. 2, first column). Increasing the speed of the target (Fig. 1) onto which the fibers were deposited resulted in an increasingly oriented fiber alignment, with a near complete alignment achieved at the highest speeds examined (Fig. 2, last column). Analyzing the number of fibers falling within ± 20 degrees of

NIH-PA Author Manuscript

NIH-PA Author Manuscript

NIH-PA Author Manuscript

the prevailing fiber direction revealed that when stationary, 33% of fibers were within this range. When the linear speed of the target was increased through 1.3, 4.0, 6.6, and 9.3 meters/second, 42.8%, 71.9%, 78.8%, and 94.0% of fibers were directed along this direction, respectively (Fig. 2). Measurement of fiber diameter at production extremes (0 and 9.3 m/s) showed only modest changes [0 m/s: 438±156 nm (min: 256, max: 821); 9.3 m/s: 519±127 nm (min: 287, max: 748)], suggesting that rotation results in alignment without further drawing.

Fiber alignment had a profound effect on the mechanical properties of scaffolds. Non-aligned scaffolds (produced at 0 m/s) had a tensile modulus of 2.1 ± 0.4 MPa (Fig. 3, heavy dotted line, n=3). At 0.3 m/s, a modest increase in tensile modulus to 2.6 ± 0.4 was observed for scaffolds cut parallel to the rotation direction (not significant vs. nonaligned, $p>0.2$). Interestingly, scaffolds produced at this speed excised perpendicular to the rotation direction showed a greater than 3-fold decrease in the tensile modulus, to 0.7 ± 0.2 MPa, a value lower than non-aligned scaffolds and those produced at the same speed excised parallel to the rotation direction (Fig. 3, $p<0.025$). This anisotropy became more pronounced at higher speeds, with a >8-fold increase in modulus parallel compared to perpendicular to the spinning direction at 4.0 m/s (Fig. 3, $p<0.001$), and a >33-fold enhancement of parallel compared to perpendicular modulus when spinning was carried out at 8.0 m/s (Fig. 3, $p<0.001$). At these higher speeds of 4.0 and 8.0 m/s, scaffold tensile moduli in the parallel direction were 7.2 ± 0.6 and 11.6 ± 3.1 MPa, respectively. In the parallel direction, each step of increasing speed led to scaffolds with higher tensile moduli (Fig. 3, $p<0.001$). Scaffold density did not vary between low and moderate speeds (0.3 and 4 m/s), while there was a small (~20%) increase at the highest speed (Table 1, $p<0.005$). Yield strain decreased while yield stress increased for increasingly aligned fibers (Table 1). Interestingly, higher speeds also resulted in lower ultimate strains for fibers excised parallel to the rotation direction. Specifically, fibers spun at 0.3 m/s yielded but did not fail with up to 70% elongation, while the 4 m/s group failed at 55±6 % and those produced at 8 m/s failed at a significantly smaller 39±4 % (data not shown, $p<0.02$). These findings suggest that increasing target speed enhances properties in the fiber direction, but predisposes the scaffold to yield and/or failure at lower strain levels as all fibers are engaged from the outset of deformation.

To better understand the properties of fiber-aligned scaffolds, a simple elastic model was generated in which position was allowed to vary within a defined width, and fiber angle was permitted to vary randomly within a range of allowable angles. Two cases were examined: a Free model, where fibers that exit the mesh over its gauge length do not contribute to overall stiffness, and a Bound model, where fiber interactions allow each fiber to contribute according to its directionality. The results of this model are shown in Fig. 4. A distinct profile in apparent stiffness is observed for each case with the transition from fully aligned (0°) to random (±90°) allowable angle conditions. In the Bound model, stiffness slowly decreased by 38%, while in the Free model, stiffness rapidly decreased by as much as 92.5% with increasing fiber dispersion. When experimental data was plotted on a separate axis over the same range of allowable angles, the shape of the curve approximated that of the Free model, suggesting few interactions occur between fibers in these scaffolds.

Fiber orientation also influenced the morphology and cytoskeleton of cells on these scaffolds. Human MSCs attached to scaffolds over a 24-hour period, with alignment and actin organization dictated by the prevailing nanofiber orientation (Fig. 5). When seeded on scaffolds produced at 0.3 m/s, cells formed contacts with multiple fibers and exhibited a pyramidal morphology, with randomly oriented actin filaments. With increasing rotation speed, fewer cellular protrusions were observed, cells were more elongated, and larger actin bundles parallel to the axis of cell elongation were observed. At the highest speed, 8.0 m/s, cells had very few protrusions and aligned continuously along a single fiber. In a longer term study, meniscus fibrochondrocytes attached to scaffolds (produced at 8.0 m/s) and showed a clear cell polarity

NIH-PA Author Manuscript

NIH-PA Author Manuscript

NIH-PA Author Manuscript

with the fiber direction after 24 hours (Fig. 6, left). After 28 days, these cells had proliferated to fill the scaffold while maintaining the alignment dictated by the scaffold architecture (Fig. 6, right).

With the recognition that many tissues, such as meniscus, intervertebral disc, and myocardium will require different alignments through the depth of a 3D construct, we explored the creation of 3D multi-layered nanofibrous structures that had different initial fiber alignments on distinct planes. To accomplish this goal, aligned fibers were accumulated on one plane, after which the scaffold was rotated relative to the shaft direction by 90°, and a further aligned layer was deposited. Micrographs of the resulting scaffolds demonstrated a clear alignment that differed by 90° between the two layers (Fig. 7).

4. Discussion

Electrospinning is not a new technology; the first patent on this topic was issued in the 1930s for textiles (Formhals, 1934). This technology has, however, found new application in the generation of tissue engineering scaffolds (reviewed in (Li et al., 2005b)). Recent advances have centered on expanding the repertoire of polymers that can be electrospun, as well as in the arrangement of deposited nanofibers (Li et al., 2005a, Theron et al., 2001). In this study, we demonstrate that by controlling the speed of the rotating target onto which nanofibers are electrospun, one can dictate the degree of fiber anisotropy within a forming scaffold. This fiber architecture in turn defines the scaffold mechanical properties, allowing for scaffolds of the same composition to be tuned to a particular stiffness. Such scaffolds can be formed with a range of anisotropies, from ~3 fold difference in tensile moduli parallel and perpendicular to the rotation direction at slower speeds to a greater than 30-fold difference at the highest speeds examined. These findings suggest that 3D nanofibrous micro-patterns can be formed with a prescribed and controllable mechanical anisotropy for the engineering of fiber-reinforced tissues of the musculoskeletal system.

In addition to measuring the mechanical properties of nanofibrous scaffolds, a simple spring model was developed to explore changing properties with respect to underlying fiber orientation. This model was formulated with two alternative conditions, that of complete fiber interaction resulting from entanglements and frictional interactions (Bound model), or the case of fiber independence (Free model) where fibers exiting the mesh do not participate in the mechanical properties. A number of simplifying assumptions were made in the model, including the lack of curvature of nanofibers, the linearity of force-elongation response of individual fibers, and the homogeneity in fiber size at different speeds. This last concern is perhaps most pressing, as it has been reported that single nanofibers of the same composition but different diameters have distinct material properties (Tan et al., 2005). Nevertheless, this simple model predicted a relationship between apparent stiffness of the scaffold and the allowable fiber dispersion angle, with the Free model showing rapid decreases with increasing fiber dispersion. When experimental data garnered from random and parallel fiber-aligned nanofiber scaffolds were plotted along with model predictions, these data were found to replicate the form, if not the magnitude, of the Free model. At its limit, this Free model predicts that with complete alignment, scaffold stiffness can be increased as much as 10-fold compared to randomly aligned meshes. This variation, coupled with the ability to choose from a variety of polymer constituents, each with its own mechanical properties (Li et al., 2006), suggests that a wide range of properties can be achieved in fiber-aligned nanofibrous scaffolds.

One of the considerable challenges remaining in the field of tissue engineering is to produce a construct with an anatomically correct architectural framework, both in terms of cell morphology and matrix deposition. In 3D, fibroblast-contracted collagen gels develop defined cellular and collagen organization with changing boundary conditions (Girton et al., 2002;

NIH-PA Author Manuscript

NIH-PA Author Manuscript

NIH-PA Author Manuscript

Henshaw et al., 2006; Thomopoulos et al., 2005). While useful as a model for neo-tissue formation, these gelatinous scaffolds do not possesses physiologic mechanical properties, and are therefore not suitable for direct implantation. The fiber-aligned nanofibrous scaffolds created in this study were found to possess controllable anisotropic mechanical properties and to dictate cellular morphology, with cell polarity following the prevailing fiber direction. Under conditions of maximal fiber-alignment, meniscal fibrochondrocytes attached to these scaffolds and their directionality was prescribed in both the short- and long-term culture. It has previously been shown in organized monolayer cultures that fibroblasts deposit an organized ECM according to cell orientation (Wang et al., 2003), and that ligament fibroblasts on an aligned nanofibrous meshes produce more collagen than on random meshes (Lee et al., 2005). It is therefore hypothesized that by creating an initial architecture, newly formed ECM will be deposited along the prescribed fiber direction in greater amounts in these nanofibrous scaffolds, expediting the formation of a neo-tissue with enhanced functional characteristics.

While these aligned scaffolds have direct application in the engineering of tissues with one prevailing fiber direction, such as muscles, tendons, and ligaments, further alterations in the production process may be well suited for other musculoskeletal applications. For example, gradually increasing the speed of rotation over the time course of production may produce depth-dependent alterations in fiber alignment, as is seen in articular cartilage (with its diffuse collagen alignment in the middle zone and highly aligned superficial layer (Mow et al., 1999)). Furthermore, changing the orientation of the forming scaffold with respect to the rotation direction may be used to create multi-layered scaffolds with a controlled, layer-dependent fiber-alignment pattern. Such three-dimensional micro-patterns provide a useful architectural framework for the generation of complex multi-lamellar tissues such as the meniscus, myocardium, or the intervertebral disc.

In summary, this study demonstrates that by dictating fiber architecture, one may readily produce a nanofibrous scaffold with controllable and anisotropic properties. By coupling this fabrication strategy with the appropriate choice of a polymer, scaffolds possessing a wide range of mechanical properties may be produced. Such scaffolds, whose composition would prescribe native mechanical properties while still providing for controlled degradation, will serve as a three-dimensional template for new tissue formation after implantation. Furthermore, by matching the mechanical properties to *in vivo* demands, these scaffolds may restore function while providing an interface for new tissue formation. By tailoring these fiber-aligned meshes to the appropriate musculoskeletal application, these scaffolds have the potential to provide both a structural and functional mimic of the native tissue through intelligent biomaterial scaffold design, enhancing the time course and functional outcome of endogenous tissue repair.

Acknowledgements

This study was supported by the Intramural Research Program of NIAMS, NIH (ZO1 AR41131). The authors gratefully acknowledge Dr. Paul Manner, George Washington University, for providing human tissue, and Gary Melvin, Office of Science and Technology, NIAMS, for instrumentation assistance.

References

Fithian DC, Kelly MA, Mow VC. Material properties and structure-function relationships in the menisci. Clinical Orthopaedics and Related Research 1990;252:19–31. [PubMed: 2406069]

Formhals, A. Process and apparatus for preparing artificial threads. United States Patent. 1,975,504. 1934.

Girton TS, Barocas VH, Tranquillo RT. Confined compression of a tissue-equivalent: collagen fibril and cell alignment in response to anisotropic strain. Journal of Biomechanical Engineering 2002;124:568–575. [PubMed: 12405600]

Haynesworth SE, Goshima J, Goldberg VM, Caplan AI. Characterization of cells with osteogenic potential from human marrow. Bone 1992;13:81–88. [PubMed: 1581112]

NIH-PA Author Manuscript

NIH-PA Author Manuscript

NIH-PA Author Manuscript

Henshaw DR, Attia E, Bhargava M, Hannafin JA. Canine ACL fibroblast integrin expression and cell alignment in response to cyclic tensile strain in three-dimensional collagen gels. Journal of Orthopaedic Research 2006;24:481–490. [PubMed: 16453340]

Huang, C-Y.; Stankiewicz, A.; Ateshian, GA.; Flatow, EL.; Bigliani, LU.; Mow, VC. Tensile and compressive stiffness of human glenohumeral cartilage under finite deformation. Proceedings of Bioengineering Conference, ASME, BED 42; 1999. p. 469-470.

Lee CH, Shin HJ, Cho IH, Kang YM, Kim IA, Park KD, Shin JW. Nanofiber alignment and direction of mechanical strain affect the ECM production of human ACL fibroblast. Biomaterials 2005;26:1261–1270. [PubMed: 15475056]

Li D, Ouyang G, McCann JT, Xia Y. Collecting electrospun nanofibers with patterned electrodes. Nano Letters 2005a;5:913–916. [PubMed: 15884893]

Li WJ, Cooper JA, Mauck RL, Tuan RS. Fabrication and characterization of six electrospun poly(alpha-hydroxy ester) based fibrous scaffolds for tissue engineering application. Acta Biomaterialia 2006;2:377–385. [PubMed: 16765878]

Li WJ, Danielson KG, Alexander PG, Tuan RS. Biological response of chondrocytes cultured in three-dimensional nanofibrous poly(epsilon-caprolactone) scaffolds. Journal of Biomedical Materials Research A 2003;67:1105–1114.

Li WJ, Laurencin CT, Caterson EJ, Tuan RS, Ko FK. Electrospun nanofibrous structure: a novel scaffold for tissue engineering. Journal of Biomedical Materials Research 2002;60:613–621. [PubMed: 11948520]

Li WJ, Mauck RL, Tuan RS. Electrospun nanofibrous scaffolds: production, characterization, and applications for tissue engineering and drug delivery. Journal of Biomedical Nanotechnology 2005b;1:259–275.

Lynch HA, Johannessen W, Wu JP, Jawa A, Elliott DM. Effect of fiber orientation and strain rate on the nonlinear uniaxial tensile material properties of tendon. Journal of Biomechanical Engineering 2003;125:726–731. [PubMed: 14618932]

Mauck RL, Soltz MA, Wang CC, Wong DD, Chao PH, Valhmu WB, Hung CT, Ateshian GA. Functional tissue engineering of articular cartilage through dynamic loading of chondrocyte-seeded agarose gels. Journal of Biomechanical Engineering 2000;122:252–260. [PubMed: 10923293]

Mow VC, Guo XE. Mechano-electrochemical properties of articular cartilage: their inhomogeneities and anisotropies. Annual Review of Biomedical Engineering 2002;4:175–209.

Mow VC, Wang CC, Hung CT. The extracellular matrix, interstitial fluid and ions as a mechanical signal transducer in articular cartilage. Osteoarthritis and Cartilage 1999;7:41–58. [PubMed: 10367014]

Noth U, Osyczka AM, Tuli R, Hickok NJ, Danielson KG, Tuan RS. Multilineage mesenchymal differentiation potential of human trabecular bone-derived cells. Journal of Orthopaedic Research 2002;20:1060–1069. [PubMed: 12382974]

Petersen W, Tillmann B. Collagenous fibril texture of the human knee joint menisci. Anatomy and Embryology Berlin 1998;197:317–324.

Proctor CS, Schmidt MB, Whipple RR, Kelly MA, Mow VC. Material properties of the normal medial bovine meniscus. Journal of Orthopaedic Research 1989;7:771–782. [PubMed: 2677284]

Riesle J, Hollander AP, Langer R, Freed LE, Vunjak-Novakovic G. Collagen in tissue-engineered cartilage: types, structure, and crosslinks. Journal of Cellular Biochemistry 1998;71:313–327. [PubMed: 9831069]

Setton LA, Guilak F, Hsu EW, Vail TP. Biomechanical factors in tissue engineered meniscal repair. Clinical Orthopaedics and Related Research 1999;367:S254–S272. [PubMed: 10546651]

Soltz MA, Ateshian GA. Experimental verification and theoretical prediction of cartilage interstitial fluid pressurization at an impermeable contact interface in confined compression. Journal of Biomechanics 1998;31:927–934. [PubMed: 9840758]

Soltz MA, Ateshian GA. A Conewise Linear Elasticity mixture model for the analysis of tension-compression nonlinearity in articular cartilage. Journal of Biomechanical Engineering 2000;122:576–586. [PubMed: 11192377]

Tan EP, Ng SY, Lim CT. Tensile testing of a single ultrafine polymeric fiber. Biomaterials 2005;26:1453–1456. [PubMed: 15522746]

NIH-PA Author Manuscript

NIH-PA Author Manuscript

NIH-PA Author Manuscript

Theron A, Zussman E, Yarin AL. Electrostatic field-assisted alignment of electrospun nanofibres. Nanotechnology 2001;12:384–390.

Thomopoulos S, Fomovsky GM, Holmes JW. The development of structural and mechanical anisotropy in fibroblast populated collagen gels. Journal of Biomechanical Engineering 2005;127:742–750. [PubMed: 16248303]

Wang JH, Jia F, Gilbert TW, Woo SL. Cell orientation determines the alignment of cell-produced collagenous matrix. Journal of Biomechanics 2003;36:97–102. [PubMed: 12485643]

Woo SL, Akeson WH, Jemmott GF. Measurements of nonhomogoeneous, directional mechanical properties of articular cartilage in tension. Journal of Biomechanics 1976;9:785–791. [PubMed: 1022791]

NIH-PA Author Manuscript

NIH-PA Author Manuscript

NIH-PA Author Manuscript

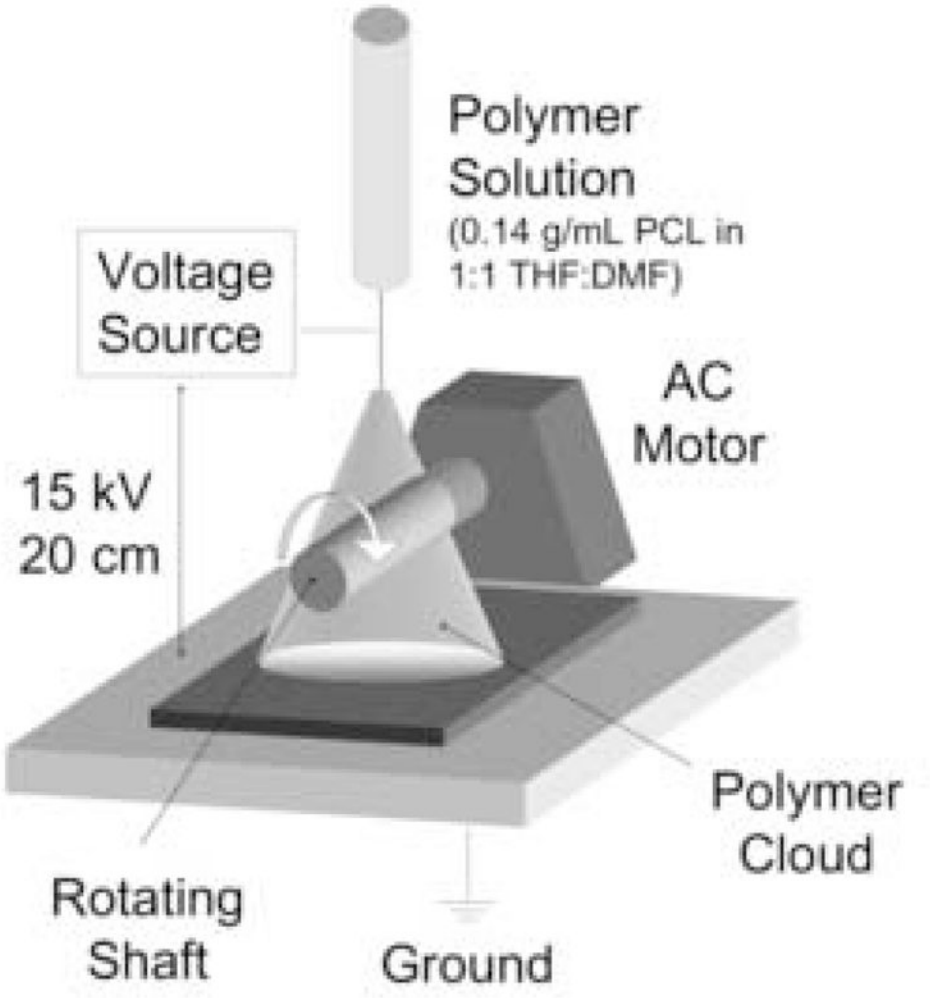

Figure 1.
Schematic of electrospinning device used to generate fiber-aligned scaffolds with the incorporation of a rotating shaft. Fibers were drawn from an 18 gauge needle through a voltage gradient of 0.75 V/cm to a grounded rotating aluminum shaft.

NIH-PA Author Manuscript

NIH-PA Author Manuscript

NIH-PA Author Manuscript

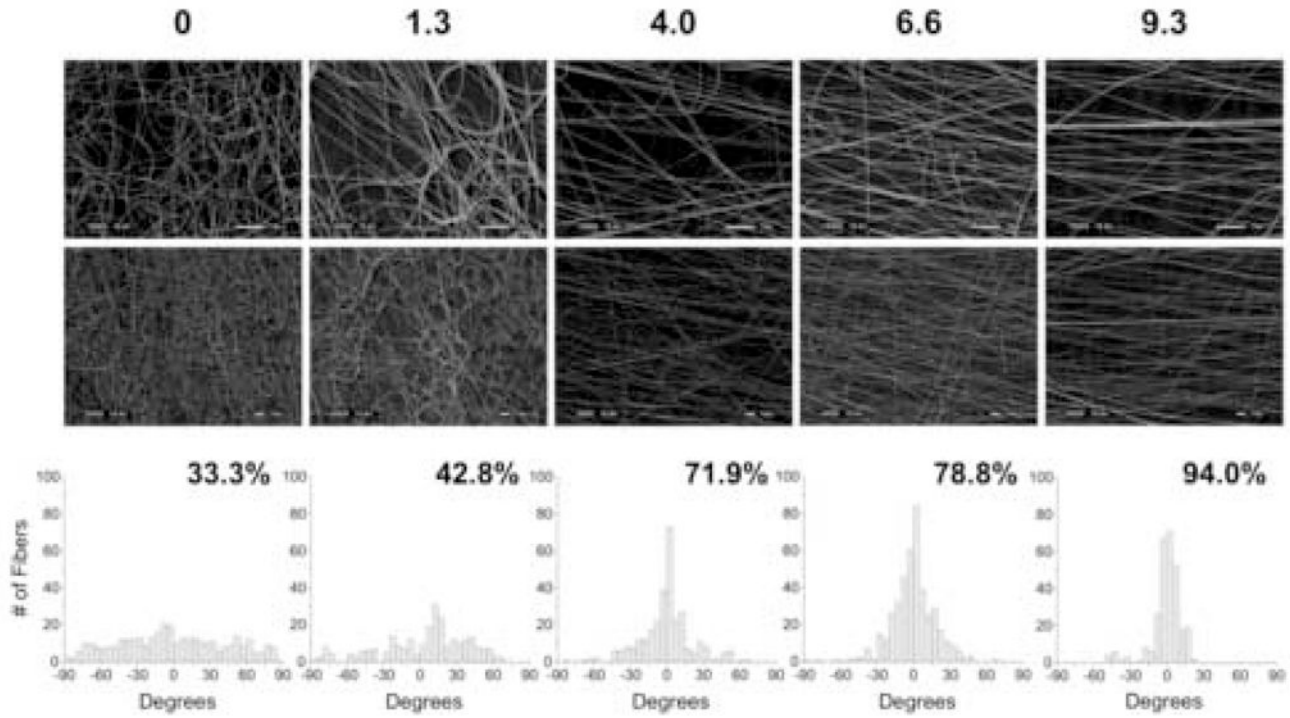

Figure 2.

Analysis of electrospun nanofiber alignment as a result of deposition onto a rotating surface. (Top) SEM micrographs (1500X and 500X) of electrospun PCL nanofibers deposited onto a rotating shaft (Scale bar: 10 μm). Linear speed of shaft was varied between 0 and 9.3 m/s and fibers were deposited for a period of 2 minutes. (Bottom) Histograms showing increases in fiber alignment with increasing rotation speed. Images were processed by overlaying a grid and measuring the angle of inclination of the fiber at each grid intersection relative to the horizontal. Each angle measurement was plotted in bins (5°/bin, >350 measurements/image). Percentage alignment was defined as the fraction of fibers falling within region between ±20 degrees to the horizontal (0°).

NIH-PA Author Manuscript

NIH-PA Author Manuscript

NIH-PA Author Manuscript

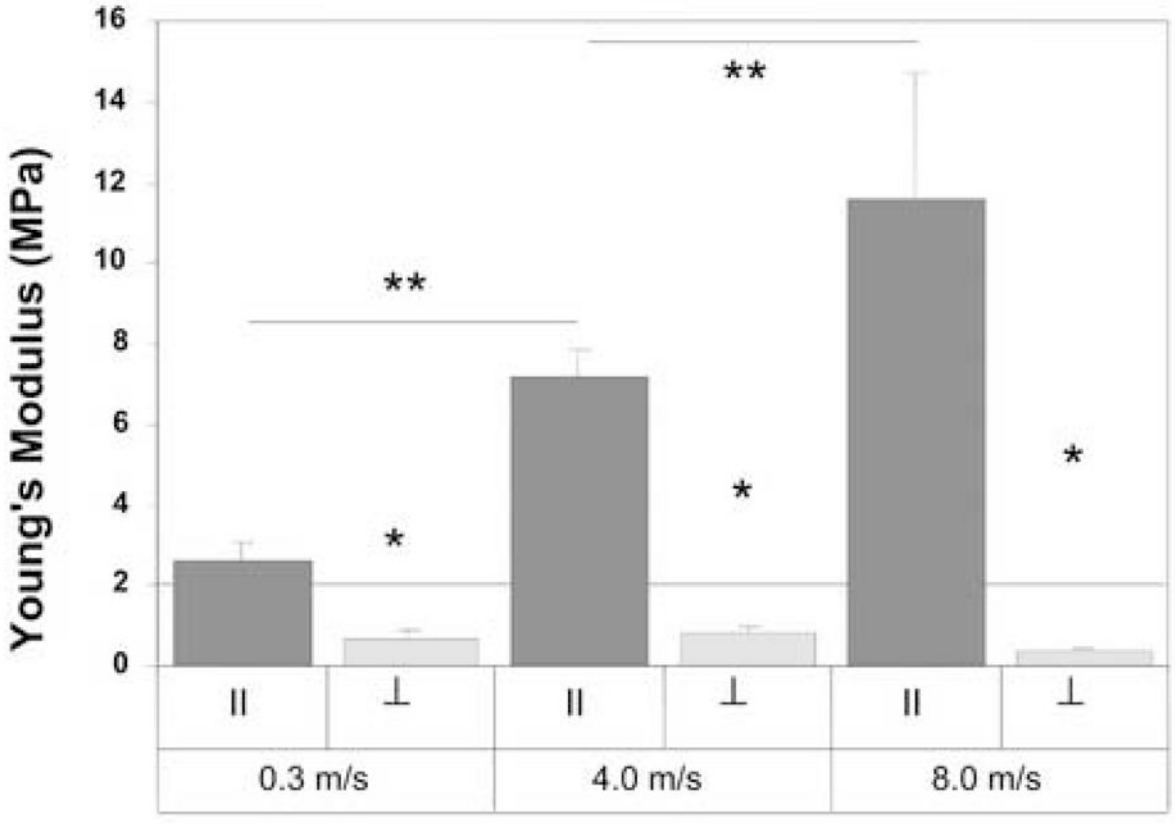

Figure 3.

Tensile Young's modulus of fiber-aligned scaffolds produced at varying speeds tested parallel (presumed fiber direction, ∥) and perpendicular (⊥) to the direction of shaft rotation. For each condition, the Young's modulus was derived from the linear region of the stress-strain curve. A total of six to eight samples were tested from two different scaffold production runs (*$p<0.05$ vs. parallel at the same speed, **$p<0.05$ vs. parallel fibers produced at different speeds).

NIH-PA Author Manuscript

NIH-PA Author Manuscript

NIH-PA Author Manuscript

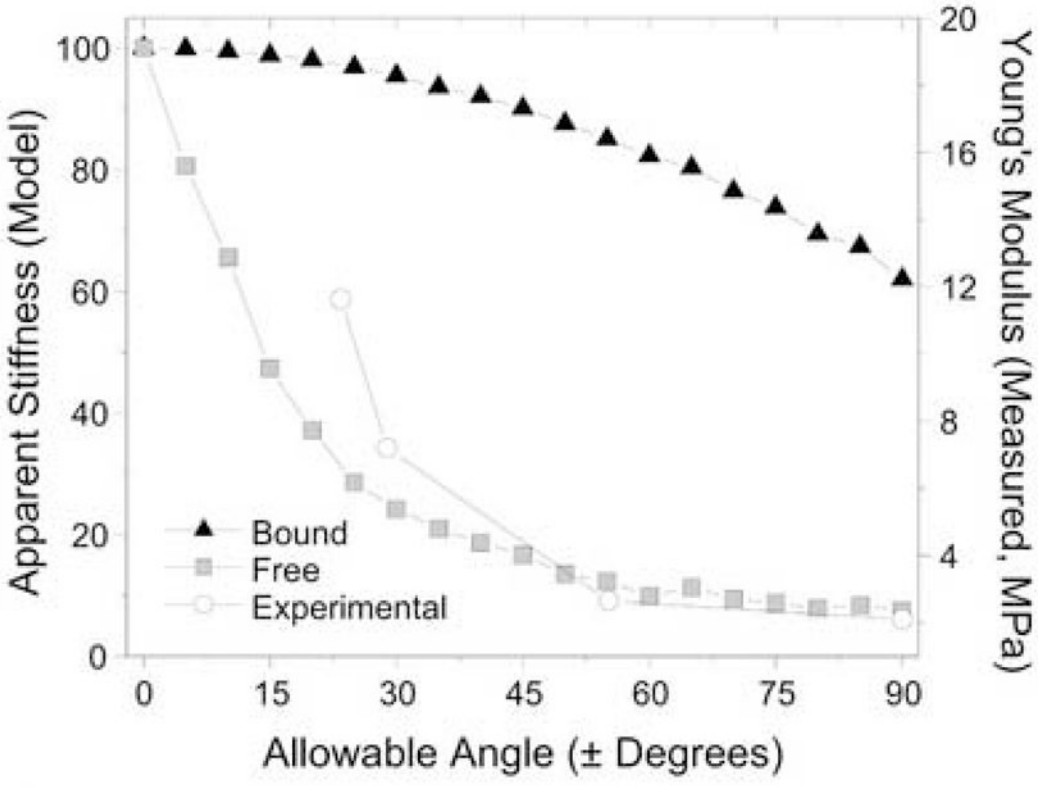

Figure 4.

Model prediction and measured mechanical properties of fiber-aligned nanofibrous scaffolds. A simple model was constructed to explore the apparent stiffness of meshes with a range of allowable fiber angles with (Bound) and without (Free) interactions between individual fibers. These model data suggest a rapid change in mechanical properties with a restriction of the fiber angles in nanofibrous scaffolds, with measured properties suggesting that the formed scaffolds act according to the Free model.

NIH-PA Author Manuscript

NIH-PA Author Manuscript

NIH-PA Author Manuscript

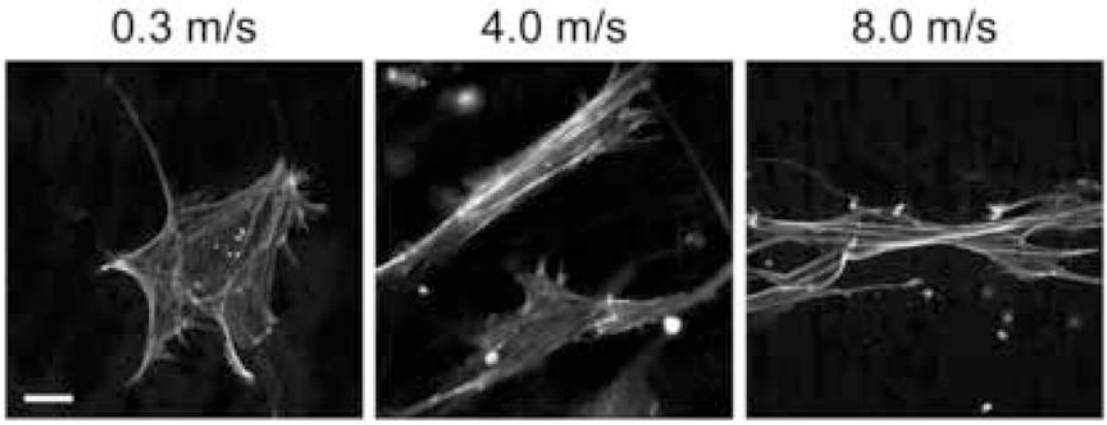

Figure 5.
Laser confocal microscopy images of filamentous actin staining in human mesenchymal stem cells (hMSCs) seeded for 24 hours on fiber aligned scaffolds formed at different rotation speeds. hMSCs seeded on increasingly aligned scaffolds showed increased cellular alignment and formation of large stress fiber bundles. Scale bar: 10 μm.

NIH-PA Author Manuscript

NIH-PA Author Manuscript

NIH-PA Author Manuscript

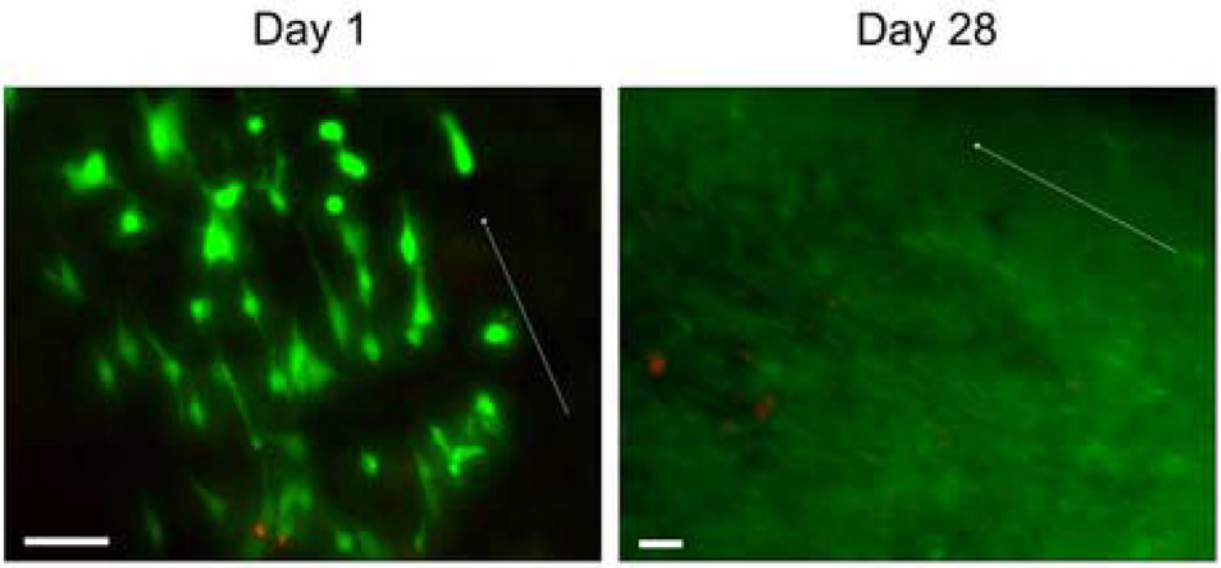

Figure 6.
Live/Dead staining of meniscal fibrochondrocytes seeded on aligned scaffolds (produced at 8.0 m/s) on day 1 and day 28. After both 1 and 28 days, initial fiber architecture of the scaffold defined the polarity and morphology of the cell population. Arrow indicates fiber direction and cell alignment. Scale bar: 50 μm.

NIH-PA Author Manuscript

NIH-PA Author Manuscript

NIH-PA Author Manuscript

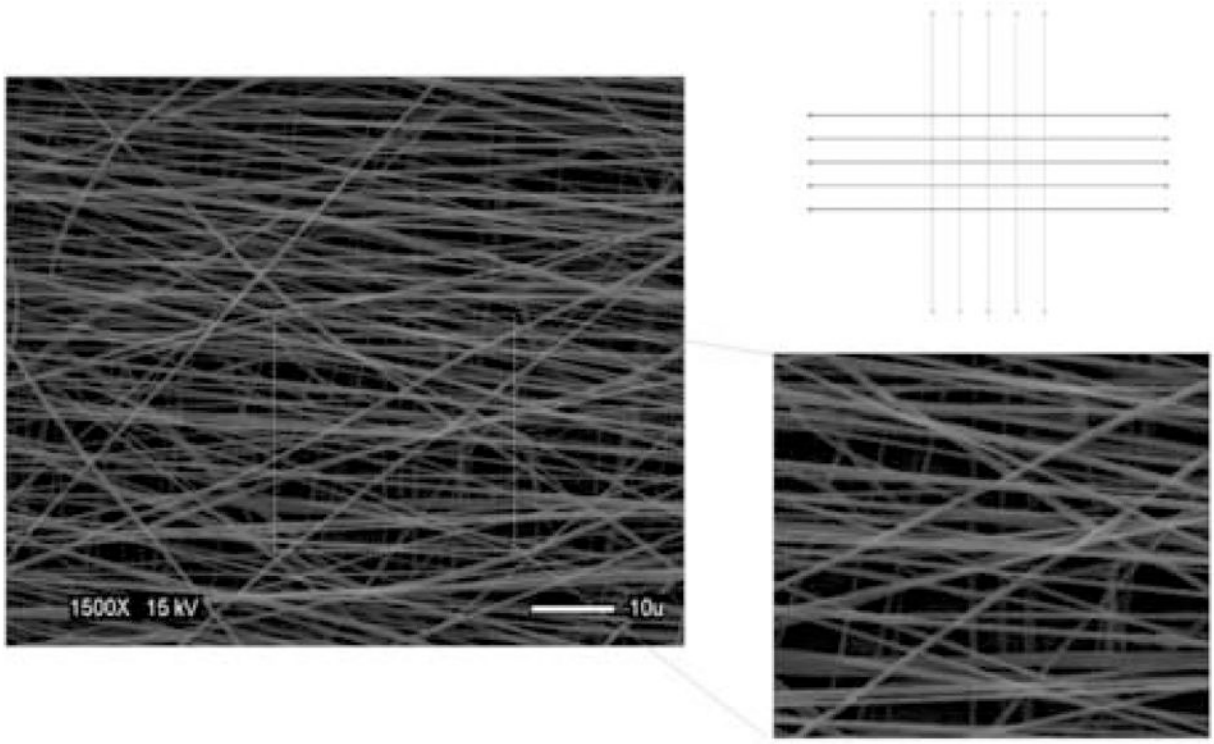

Figure 7.
Schematic (grey lines, lower level; black lines, upper level) and SEM photomicrograph of multi-laminar fiber-aligned scaffold showing distinct alignment in different layers. This scaffold was produced by electrospinning onto a rotating shaft (9.3 m/s) for 2 minutes followed by a 90° turn of the deposited mesh and a further electrospinning period (9.3 m/s) for 2 minutes (Image acquired at 1500X, 15kV). Scale bar: 5 μm.

NIH-PA Author Manuscript NIH-PA Author Manuscript NIH-PA Author Manuscript

Table 1

Properties of fiber-aligned nanofibrous scaffolds

Rotation Speed(m/s)	0.3		4.0		8.0	
Fiber Direction	∥	⊥	∥	⊥	∥	⊥
Yield Strain (ε_Y, %)	**18.7*** 3.9	**23.6** 3.82	**13.9*** 3.6	**23.4** 0.92	**9.7***,‡ 0.06	**35.2** 1.8
Yield Stress (σ_Y, MPa)	**0.48*** 0.10	**0.16** 0.05	**0.91***,‡ 0.24	**0.16** 0.02	**1.03***,‡ 0.20	**0.08** 0.00
Density (ρ, gm/cm^3)	**0.101** 0.010	**0.100** 0.011	**0.102** 0.009	**0.105** 0.009	**0.123**$^{+}$ 0.007	**0.126**$^{+}$ 0.005

Yield points were determined from the intersection of a line shifted 0.5% strain from the origin, with a slope corresponding to the measured Young's modulus for each fiber. ∥ indicates fibers excised parallel to rotation direction, ⊥ indicates scaffolds excised perpendicular to rotation direction. Data are reported as the mean (upper bold number) and standard deviation (lower number) for 3–4 samples from one fiber production.

*indicates $p<0.05$ vs. perpendicular sample at same speed

$^{+}$indicates $p<0.005$ vs. same group formed at 0.3 and 4 m/s

‡indicates $p<0.01$ vs. same group formed at 0.3 m/s